Analytica Chimica Acta 1226 (2022) 340265

Contents lists available at ScienceDirect

Analytica Chimica Acta

journal homepage: www.elsevier.com/locate/aca

Photoelectrochemical biosensor based on CdS quantum dots anchored h-BN nanosheets and tripodal DNA walker for sensitive detection of miRNA-141

Fengyi Wang [a,1], Yaqi Liu [a,1], Lu Zhang [a], Zuhao Zhang [a], Chuan Huang [a], Dejin Zang [b,**], Haiqing Wang [a,***], Shenguang Ge [a,*], Jinghua Yu [c]

[a] Institute for Advanced Interdisciplinary Research, University of Jinan, Jinan, 250022, PR China
[b] Institute of Materia Medica, Shandong First Medical University & Shandong Academy of Medical Sciences, Jinan, 250117, PR China
[c] School of Chemistry and Chemical Engineering, University of Jinan, Jinan, 250022, PR China

HIGHLIGHTS

- Porous h-BN nanosheets gave large specific surface areas and extensive active reaction sites.
- CdS quantum dots anchored porous h-BN nanosheets as photoelectric materials to accomplish signal amplification.
- Catalytic hairpin assembly and the tripodal DNA walker cascade signal amplification improved the sensitivity.

GRAPHICAL ABSTRACT

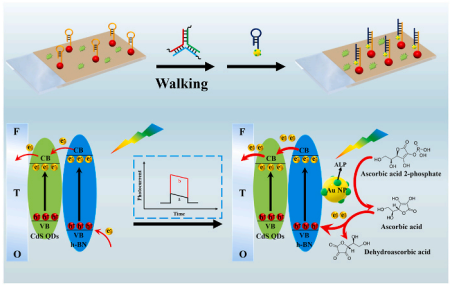

ARTICLE INFO

Keywords:
Photoelectrochemical
Tripodal DNA walker
h-BN nanosheets
CdS quantum Dots
MicroRNA-141

ABSTRACT

Herein, a high-sensitivity photoelectrochemical (PEC) biosensor was developed based on CdS quantum dots (QDs) sensitized porous hexagonal boron nitride (h-BN) nanosheets (NSs) and the multiple sites tripodal DNA walker (TDW) formed by catalytic hairpin assembly (CHA). Noticeably, the porous structure of h-BN NSs gives it a lasting gift of large specific surface areas and extensive active reaction sites, which makes it possible to be employed as photoelectric substrate material. The h-BN/CdS QDs composite material promotes the transmission of photogenerated electrons and holes, the outstanding photoelectric conversion efficiency. Meanwhile, the CHA-formed TDWs triggered by miRNA-141 moved on track strand-functionalized electrode, so that a large number of alkaline phosphatase (ALP) was immobilized on the electrode surface and further in situ catalyzed ascorbic acid 2-phosphate (AAP) to produce ascorbic acid (AA) as the electron donor. As the result of the decisive influence of electron donor on PEC biosensor, the sensitive detection of miRNA-141 was realized. The proposed PEC biosensor displayed an excellent linear relationship ranging from 1 fM to 100 nM with a detection limit of 0.73 fM, providing a powerful strategy for early clinical diagnosis and biomedical research.

* Corresponding author.
** Corresponding author.
*** Corresponding author.
E-mail addresses: zangdejin_lm@163.com (D. Zang), ifc_wanghq@ujn.edu.cn (H. Wang), chm_gesg@163.com (S. Ge).
[1] F. W. and Y. L. contributed equally to this paper.

https://doi.org/10.1016/j.aca.2022.340265
Received 14 July 2022; Received in revised form 9 August 2022; Accepted 12 August 2022
Available online 17 August 2022

1. Introduction

MicroRNAs (miRNAs) are nucleotides involved in gene regulation whose abnormal expression result in diseases such as cancer, tumors, neurological diseases and cardio-cerebrovascular disease. Therefore, miRNAs play a crucial role in both diagnostics and therapeutics of diseases [1–3]. For instance, microRNA-141 (miRNA-141) is a very important cancer biomarker for clinical medicine and the accurate detection of miRNA-141 ensures the pre-diagnosis, treatment and post-treatment effect of ovarian cancer, hepatocellular carcinoma and prostate cancer [4]. For the demand of precise and rapid analysis to trace miRNAs, multitudinous effective detection technologies have been proposed, such as electrochemistry (EC) [5,6], electrochemiluminescence (ECL) [7–9], chemiluminescence (CL) [10], fluorimetry (FL) [11–13] and photoelectrochemistry [14–16]. Among them, the PEC method integrates the fascinating properties of electrochemical and photochemical analysis such as high sensitivity, high selectivity and low background [17,18]. The amplification of photoelectric signal is one of the critical factors to decide the sensitivity of PEC detection, so the development of highly active photosensitive composites have always been a research focus [19]. Notably, the outstanding photocurrent response benefits from the wide light absorption range, the fast transfer of charges and the suppression of photogenerated electron-hole coincidence [20].

Hexagonal boron nitride (h-BN) nanosheets (NSs), a representative of two-dimensional (2D) layered material, possesses massive specific surface areas, brilliant stability, high charge mobility and good biocompatibility, which is especially beneficial to be used as the base material of PEC biosensor [21,22]. Unfortunately, the photocurrent signal produced by pure h-BN cannot reach the analysis requirements owing to the wide band gap as well as low sunlight utilization, which urgently to be improved through the sensitizer photoelectric material [23]. CdS quantum dots (QDs), a kind of semiconductor with attractive narrow band gap, has become a significant photoactivity material due to its intense PEC property under visible light irradiation [24,25]. The combination of CdS QDs as sensitizer with h-BN effectively facilitate the separation of photoelectrons and holes, thus enhancing the photocurrent response.

For the sake of further promoting the analysis performance, diversification of amplification strategy gives the huge possibility of PEC sensors. The DNA walker is a sort of DNA nanomachine which can go forward across the DNA track autonomously and release multiple signal molecules for signal transduction or signal amplification [26,27]. The driving force of DNA walker is usually environmental stimuli, DNAzyme or endonuclease-mediated hydrolysis and the toehold-mediated strand displacement reaction (TSDR) [28]. However, DNAzyme or endonuclease are obviously affected by conditions such as temperature and pH [29]. By contrast, TSDR is an isothermal nucleic acid amplification strategy constructing DNA walker, which can achieve steady movement without being disturbed by environmental factors [30]. In addition, other types of signal amplification strategies have been applied in the PEC field to achieve high detection sensitivity, such as catalytic hairpin assembly (CHA) [31], roll circle amplification (RCA) [32,33], hybridization chain reaction (HCR) [34] and so on. CHA is a representative non-enzymatic isothermal amplification reaction, which owns the fascinating characteristic of resisting the interference of environmental factors [35].

Therefore, taking account of the above advantages, a sensitive PEC biosensor was developed with the strategy of TSDR integrating hairpin DNA to assemble TDW. With the participation of target miRNA-141, three carefully designed hairpin DNA were sequentially opened to form a three-legged DNA walker. Briefly, TDW was propelled by TSDR, moved on the track-functionalized electrode surface, and opened the hairpin DNA H4 on the modified electrode to expose its toehold region. Furthermore, the newly exposed region of H4 tended to hybridize with the alkaline phosphatase (ALP) - Au nanoparticles (Au NPs) - H5 conjugate by a strand displacement reaction, bringing about the H4/H5 double-stranded DNA composition and releasing TDW into the next walking process. For this reason, H4 was assembled as the H4/ALP- Au NPs-H5 duplex to anchor a large amount of ALP-Au NPs-H5 on the electrode surface, which realized significant PEC signal enhancement thanks to the intriguing ability of ALP to catalyze ascorbic acid 2-phosphate (AAP) to generate the electron donor ascorbic acid (AA).

2. Experimental section

2.1. Materials and apparatus

The reagents and instruments were displayed in the Supplementary Material. All biological sequences were made a list in Table S1.

2.2. Preparation of h-BN nanosheets and CdS QDs

The specific experimental process of h-BN NSs and CdS QDs were described in Supplementary Material.

2.3. Construction of the tripodal DNA walker

Initially, each kind of DNA hairpin (H1, H2, H3) was kept at 95 °C for 5 min and afterwards slowly cooled to 25 °C for at least 2 h in the cause of holding stable DNA secondary structures. The annealed DNAs were stored at 4 °C for subsequent experiments. To prepare the TDW, 10 μL of miRNA-141 with different concentrations were mixed with 5 μL of 1 nM H1, 5 μL of 1 nM H2 and 5 μL of 1 nM H3, incubated at 37 °C for 4 h. The formed stable TDW was stored at 4 °C for further experiments.

2.4. Fabrication of the biosensor

The CdS QDs/h-BN/FTO modified electrode was prepared by layer by layer self-assembly in the 2 wt % poly (diallyl dimethyl ammonium chloride) (PDDA) solution containing 0.5 M NaCl [36]. Concretely, the FTO electrode was ultrasonically cleaned with acetone, ethanol and ultrapure water for 30 min, respectively. After drying, 10 μL of h-BN solution (5 mg mL^{-1}) was dropped on the FTO electrode to turn into a film as the PEC active substrate. Then, the modified FTO electrode was alternately dipped into 2 wt % PDDA and the CdS QDs solution for 10 min and repeated in triplicate. The CdS QDs/h-BN/FTO composite electrode was obtained after carefully cleaning with ultrapure water and drying at room temperature.

For the sake of reducing disulfide bonds, H4 was deal with 10 nM Tris-HCl buffer (pH 7.4) containing 10 mM Tris (2-carboxyethyl) phosphine (TCEP) in the dark for 1h before incubation [37]. After that, 20 μL of 1 μM H4 was introduced into the modified electrode surface and kept at 4 °C for 12 h to obtain the CdS QDs-H4/h-BN/FTO. Afterwards, the nonspecific sites on the obtained electrode surface were blocked with 2 mM 6-mercapto-1-hexanol (MCH) solution for 1 h [38]. Unstable residues on the electrode surface were washed with buffer.

2.5. PEC measurement procedure

For the sake of investigating the measure property of the proposed PEC biosensor, 5 μL of TDW was introduced into the modified electrode to open H4, then continued to drop 5 μL of ALP-Au NPs-H5 and incubated for 40 min. After the above electrode was washed three times with buffer, the PEC response was tested in 10 nM Tris-HCl (pH 7.4) solution containing 0.1 M AAP.

3. Results and discussion

3.1. Characterization of h-BN nanosheets

The morphology of h-BN NSs was observed by the scanning electron

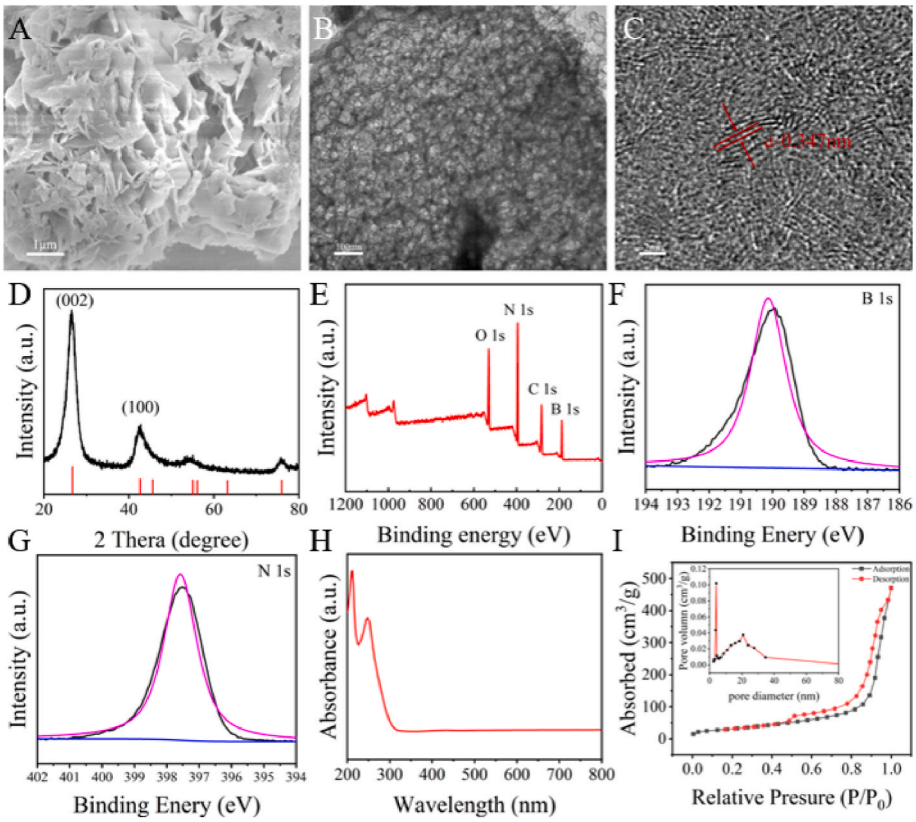

Fig. 1. (A) SEM image of h-BN. (B) TEM image of h-BN. (C) HRTEM image of h-BN. (D) XRD pattern of h-BN. (E) XPS spectra of h-BN. XPS spectra of (F) B 1s and (G) N1s of h-BN. (H) UV–vis spectra of h-BN. (I) N_2 adsorption−desorption isotherms of h-BN nanosheets.

microscopy (SEM). According to Fig. 1A, the as-fabricated h-BN exhibited a thin and lamellar structure due to the formation of gases during calcination. The microstructure of h-BN (Fig. 1B) was explored by transmission electron microscopy (TEM). The high-resolution TEM (HR-TEM) image (Fig. 1C) exhibited an excellent crystallinity with lattice spacing of 0.347 nm. Moreover, the crystal structure of as-prepared h-BN was explored by X-ray diffraction (XRD) patterns. As shown in Fig. 1D, the XRD patterns displayed the characteristic diffraction peaks at 26.7°and 42.6°, which assigned to crystal planes of (002) and (100), respectively.

The X-ray photoelectron spectroscopy (XPS) survey spectrum was applied to further investigate chemical compositions of h-BN NSs. According to Fig. 1E, the as-prepared h-BN NSs contained the four elements C, N, O and B, which were completely identical accord with the research

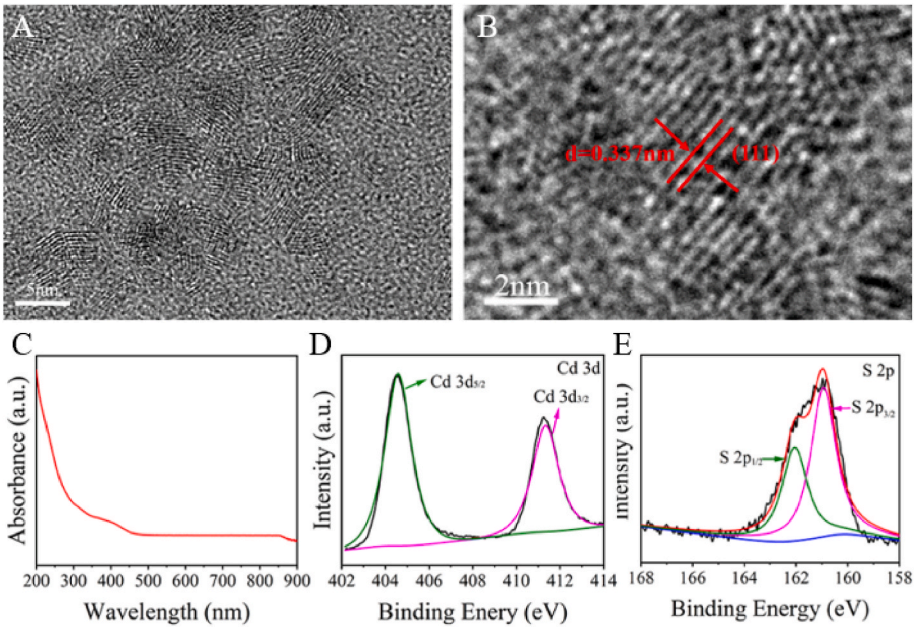

Fig. 2. (A) (B) HRTEM image of CdS QDs. (C) UV–vis spectra of CdS QDs. XPS spectra of (D) Cd 3d and (E) S 2s of CdS QDs.

results of the reported literature [39]. The signal of C 1s was taken as a reference to calibrate the binding energies to conduct charge calibration on the original data, to reduce the error caused by the instrument. The presence of O was present basically because the product absorbed oxygen from the atmospheric air during storage. As displayed in Fig. 1F, the main peak of B 1S corresponded to the B–N bond found at 190.1 eV. In addition, the high-resolution N 1s spectra signal at 398.5 eV respected to the N–B bond (Fig. 1G). To research the optical property of the h-BN, the UV–visible diffuse reflectance spectrum was used to analyze h-BN NSs. As manifested in Fig. 1H, the h-BN NSs revealed absorption in the UV region.

Furthermore, the N_2 adsorption-desorption isotherms of h-BN NSs was acquired and displayed in Fig. 1I. The Brunauer-Emmett-Teller (BET) surface area was 481.31 $cm^3\ g^{-1}$, which confirmed the porous structure of h-BN NSs. Therefore, the large specific surface area of h-BN NSs improved the utilization rate of solar energy and enhanced the absorption of light [21]. The above results implied that h-BN NSs were suitable as photoelectric substrate material for PEC biosensor.

3.2. Characterization of CdS QDS

The TEM image (Fig. 2A) showed that the prepared CdS QDs owned a single shape and uniform size, with a particle size of about 6 nm. Besides, HRTEM was applied to further track lattice fringes of CdS QDs. As exhibited in Fig. 2B, the lattice spacing of spherical CdS QDs was 0.336 nm, assigned to (111) plane implied high crystallinity. To further investigate the crystal planes of CdS QDs, the XRD pattern was shown in Fig. S1A. Compared with JCPDS PDF 41–1049, the XRD patterns matched well, with three distinct diffraction peaks at 26.4°, 43.6° and 51.8°, which were ascribed to (111), (220) and (311) respectively. Moreover, to research the optical properties of CdS QDs, the ultraviolet–visible (UV–vis) absorption and Fourier transform infrared (FT-IR) spectroscopy were put in effect to reflect the optical properties of CdS QDs. According to Fig. 2C, CdS QDs possessed strong and wide absorption at 200 nm–500 nm, indicating that it owned excellent potential as the photoelectric sensitizer. The FT-IR spectrum in Fig. S1b showed the characteristic peaks of CdS QDs at 3415.1 cm^{-1} (O–H), 1568.4 cm^{-1} (C═O) and 1402.1 cm^{-1} (C–O), meant that 3-Mercaptopropionic acid (MPA) modified CdS QDs were successfully prepared.

To further determine the valence state of CdS QDs, XPS characterization was carried out. HR-XPS spectra of Cd 3d showed two distinct characteristic peaks at 405.1 eV and 411.8 eV, which were assigned to Cd $3d_{5/2}$ and Cd $3d_{3/2}$ respectively (Fig. 2D). The photoelectron peaks for S 2p emerged at 161.5 eV and 162.5 eV, which were ascribed to the S $2p_{3/2}$ and S $2p_{3/2}$ for S^{2-} in CdS QDs (Fig. 2E).

3.3. Mechanism of the PEC biosensor

Taking the preponderance of DNA walker for signal amplification, a novel PEC biosensor coupled with TDW was assembled by target-triggered CHA enhancement strategy to detect miRNA-141. As shown in Scheme 1, the TDW was establish with three carefully designed hairpin DNA H1, H2, and H3, which was triggered by target miRNA-141 and spontaneously assembled in sequence. Notably, the 3' end of these hairpin DNA all had the same sequence (black) to ensure more efficient multipoint replacement. The CHA cycle began with the hybridization of the target miRNA-141 with hairpin DNA H1 (blue), which opened the hairpin structure to expose the toehold region of H1, and formed the double stranded structure of miRNA-141/H1. The newly exposed toehold region of H1 triggered the same reaction to open H2, which hybridized with miRNA-141/H1 to constitute miRNA-141/H1/H2. Analogously, H3 (green) was opened and exposed its toehold region in the same way, combining with the above miRNA-141/H1/H2 to assemble Y-pipe DNA H1–H2–H3 and release miRNA-141 to the next cycle. The CHA cycle did not suspend until all H1, H2 and H3 were converted to Y-pipe DNA. The Y-pipe DNA with three single strands DNA

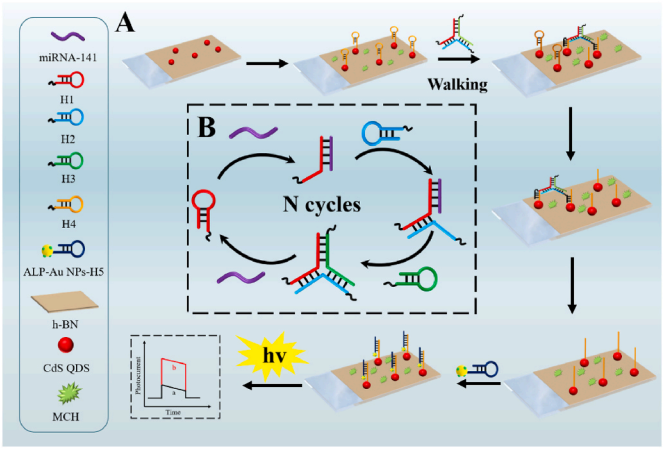

Scheme 1. (A) Schematic representation of PEC biosensor based on the CHA-formed TDW strategy for the Detection of miRNA-141; (B) Fabrication of the TDW.

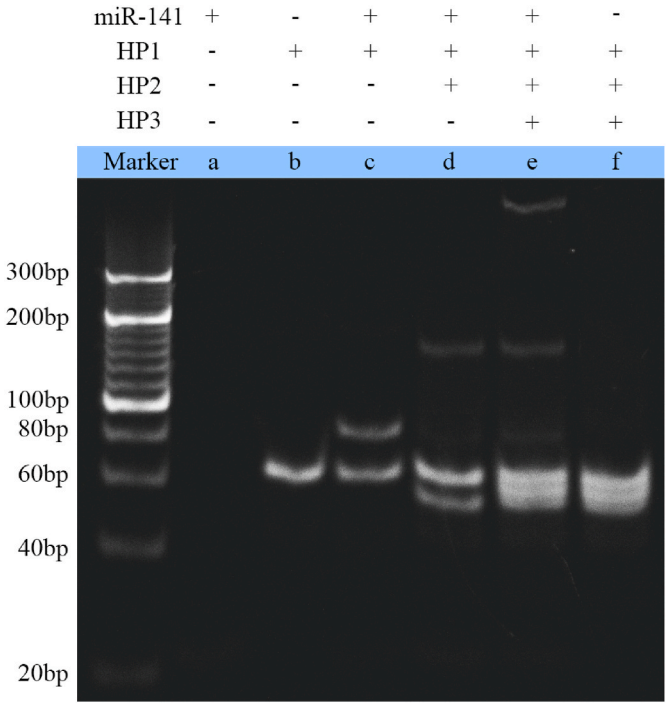

Fig. 3. Native-PAGE analysis of different samples (Lane a: 2 μM miRNA-141; Lane b: 2 μM H1; Lane c: 2 μM miRNA-141, H1; Lane d: 2 μM miRNA-141, H1, H2; Lane e 2 μM miRNA-141, H1, H2, H3; Lane f: 2 μM H1, H2, H3).

formed by CHA cycle was called TDW.

Scheme 1 showed the process of TDW continuously walking along the electrode surface to convert and accumulate signals. The h-BN/CdS QDs composite was directly anchored on the FTO electrode, and the CdS QDs modified a large amount of H4 to serve as DNA tracks. When miRNA-141 was present in the system, the CHA process was triggered to produce the TDW. The three-legged DNA walker bound to H4 on the modified electrode surface and underwent a strand displacement reaction, exposing the toe region of H4 hairpin structure. The newly exposed toe region could form a double-stranded DNA structure of H4/H5 with ALP-Au NPs-H5 through strand displacement reaction and released the DNA walker to continue walking, which anchored a large amount of ALP on the electrode surface. As expected, ALP catalyzed AAP in solution to generate AA as an electron donor to consolidate photoelectric response.

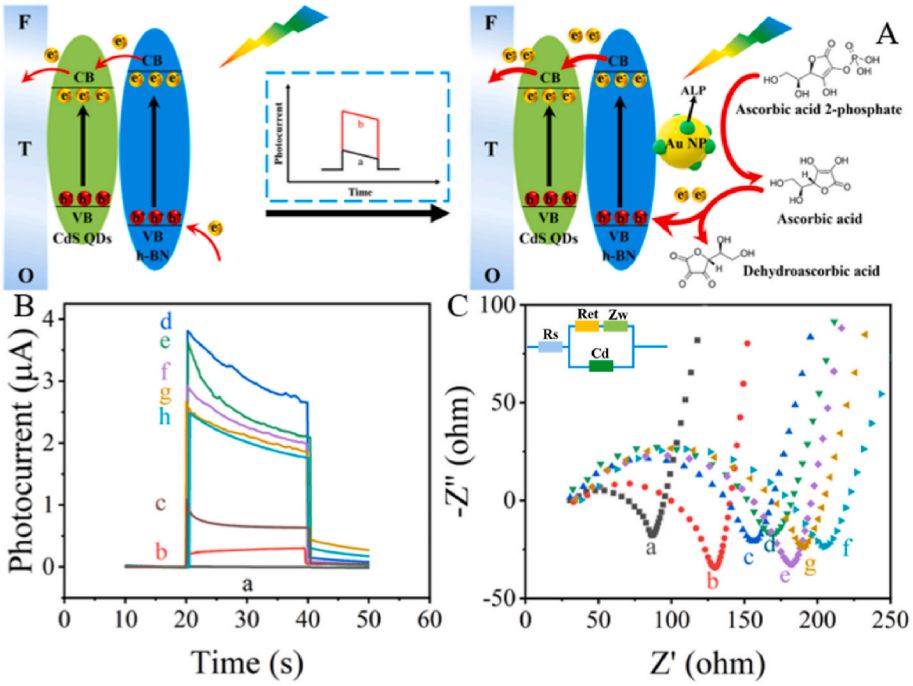

Fig. 4. (A) PEC mechanism of h-BN/CdS QDs; (B) PEC response in 10 nM Tris-HCl (pH 7.4) containing 0.1 M AA. (a) FTO; (b) h-BN/FTO; (c) CdS QDs/FTO; (d) CdS QDs/h-BN/FTO; (e) CdS QDs-H4/h-BN/FTO; (f) MCH/CdS QDs-H4/h-BN/FTO; (g) TDW/MCH/CdS QDs-H4/h-BN/FTO; (h) ALP-Au NPs-H5/MCH/CdS QDs-H4/h-BN/FTO. (C) (a) FTO; (b) h-BN/FTO; (c) CdS QDs/h-BN/FTO; (d) CdS QDs-H4/h-BN/FTO; (e) MCH/CdS QDs-H4/h-BN/FTO; (f) TDW/MCH/CdS QDs-H4/h-BN/FTO; (g) ALP-Au NPs-H5/MCH/CdS QDs-H4/h-BN/FTO. EIS in 5 mM $[Fe(CN)6]^{3-/4-}$ containing 0.1 M KCl at a bias potential of 0.19 V.

In this system, increased miRNA-141 concentration led to the enhanced ALP loading, thus raised the concentration of AA for improving photocurrent responding. Because of the in-situ generation of AA, the considerable initial photocurrent signal driven by h-BN NSs/CdS QDs and the amplification and accumulation effect of TDW, the proposed platform achieved the sensitive and specific detection of miRNA-141.

3.4. Characterization of the tripodal DNA walker

The successful assembly of TDW was vital for the designed sensing system, hence the 8% polyacrylamide gel electrophoresis (PAGE) was performed to monitor the formation of TDW. According to Fig. 3, no migration bands were observed in lane a because miRNA-141 was a short single-stranded structure. The band (a ~ e) indicated the successful progressive hybridization. It could be seen from lane g that in the

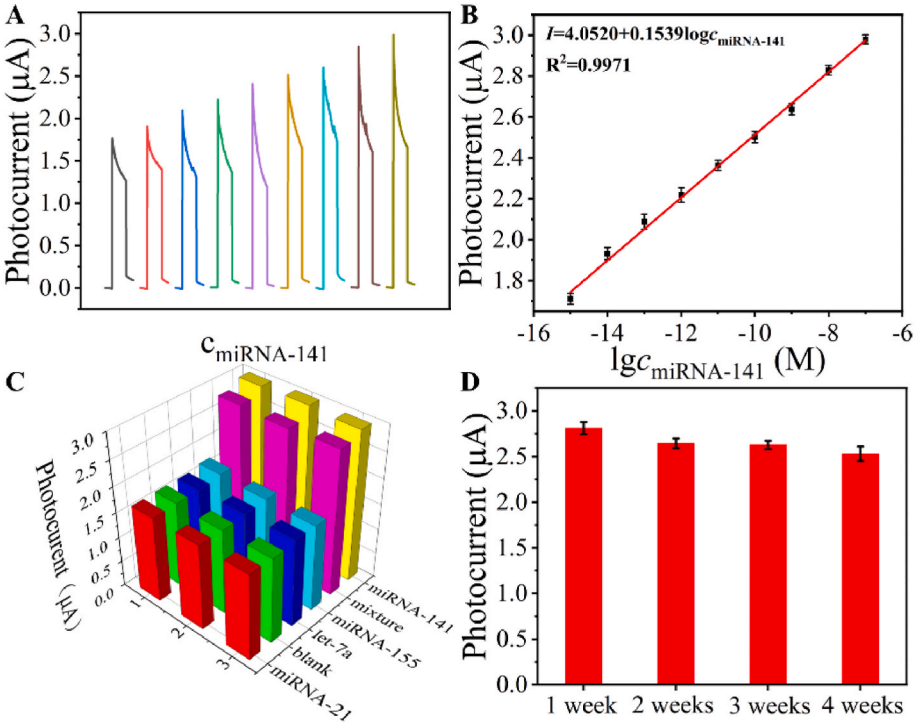

Fig. 5. (A) Photocurrent corresponding to different $c_{miRNA-141}$ (from left to right: 1 fM, 10 fM, 100 fM, 1 pM, 10 pM, 100 pM, 1 nM, 10 nM and 100 nM). (B) The linear calibration curve of the PEC biosensor. (C) Specificity of the PEC biosensor against 1 μM miRNA-21, blank, 1 μM let-7a, 1 μM miRNA-155, 100 nM miRNA-141 and mixture including all the solutions mentioned above. (D) The photocurrent response of the biosensor stored with different times (error bars show S.D., n = 3).

absence of miRNA-141, the three hairpin structures, H1, H2 and H3, did not assemble into three-legged DNA Walker. The above results proved the feasibility of CHA forming TDW in comparison lane g.

3.5. Electrochemical characterizations of PEC biosensor

Fig. 4A showed the response mechanism of PEC. h-BN NSs and CdS QDs excited photogenerated electrons (e^-) and holes (h^+) under visible light irradiation. Because of the energy level matching and close contact between h-BN and CdS QDs, the photogenerated electrons in h-BN/CdS QDs composites were shifted from valence band (VB) to conduction band (CB) after absorbing visible light, leaved holes in VB. Electrons were shifted from CB of h-BN to CB of CdS QDs and then to the electrode surface to form a stable photocurrent. The stepwise modification process of the electrode was monitored by the PEC detection and the electrochemical impedance spectroscopy (EIS) method. Fig. 4B showed the bare FTO electrode was practically without photocurrent signal (curve a). The photocurrent became larger when h-BN was modified on the FTO electrode (curve b). In addition, the photocurrent response of CdS/FTO was also enhanced. However, the CdS QDs/h-BN/FTO electrode had the largest photocurrent (curve d). As mentioned above, CdS QDs sensitized h-BN composites owned brilliant photoelectric conversion efficiency and PEC properties. As expected, when H4, MCH and TDW were continuously anchored on the modified electrode, the photocurrent response decreased in turn (curve e to g). These phenomena could be interpreted as non-conductivity and high steric hindrance of biomolecules, which inhibited electron transfer from AA to electrode surface. Then, TDW was incubated with the reaction solution containing ALP-Au NPs-H5, and the DNA walker linked ALP-Au NPs-H5 to the electrode surface by strand displacement reaction. The introduction of the relatively large volume complex further increased the steric resistance, resulting in a significant attenuation of photocurrent (curve h).

As we all know, the semicircle diameter in the Nyquist plot measured by EIS represented the interfacial electron transfer resistance (R_{et}) of the modified electrode.

Fig. 4C indicated the impedance changes associated with the modification of the FTO electrode. Due to the rapid electrons transfer of $[Fe(CN)_6]^{3-/4-}$, the bare FTO electrode exhibited minimal R_{et} (curve a). With the modification of substrate h-BN, the R_{et} value increased (curve b), which was attributed to the blocking effect of h-BN on electron transfer. The introduction of CdS QDs sensitizer led to the continued increased of R_{et}, probably due to its semiconductor properties (curve c). When the hairpin H4 was anchored on the electrode surface, the negatively charged DNA prevented the transfer between $[Fe(CN)_6]^{3-/4-}$ and the electrode interface, resulting in the expansion of R_{et} (curve d). The R_{et} was further increased due to the addition of non-conductive MCH on the electrode surface (curve e). Logically, after TDW was hybridized with H4 on the modified electrode, further increased the R_{et} value (curve f). Finally, it could be seen from the curve g that the impedance of the modified electrode was slightly reduced, which boiled down to the ALP-Au NPs -H5 replacing the TDW. The reduction of R_{et} value was mainly attributed to the preeminent conductivity of Au NPs. The above PEC and EIS results corroborated mutually, indicating the successful construction of the proposed PEC biosensor.

3.6. Detection of miRNA-141

For the sake of investigating the analytical performance of the presented PEC biosensor, a series of miRNA-141 with different concentrations were detected under optimized experimental conditions (Fig. S3). According to Fig. 5A, the corresponding photocurrent signals intensity gradually increased, while the concentration of miRNA-141 ($c_{miRNA\text{-}141}$) increased from 1 fM to 100 nM. The logarithm of $c_{miRNA\text{-}141}$ owned a good linear correspondence with the photocurrent signal intensity. According to Fig. 5B, the linear range of $c_{miRNA\text{-}141}$ was 1 fM~100 nM, and the linear regression equation was $I = 4.0520 + 0.1539 \lg c_{miRNA\text{-}141}$ with the regression coefficient (R^2) was 0.9971. Furthermore, compared with other miRNA sensors (Table S2), the proposed PEC biosensor had a low limit of detection of 0.73 fM (S/N = 3).

3.7. Specificity, repeatability and stability of the biosensor

Anti-jamming performance is a crucial factor to affect the accuracy and sensitivity of PEC biosensor. The miRNA-155, let-7a, and miRNA-21 were selected as potential disruptors for specific studies of PEC biosensors. According to Fig. 5C, the presence of target miRNA-141 or target containing mixture showed the significant increase in photocurrent, while the highly homologous interfering miRNAs or the blank sample could not set off the biological cycle to improve the photocurrent. The above results proved that the proposed PEC biosensor possessed marvellous specificity. For the sake of researching the stability, the working electrodes were placed at 4 °C for 4 weeks, and three parallel experiments were performed every week. As displayed in Fig. 5D, the photocurrent response signal was 90.09% of the initial value after 4 weeks of storage, which implied the designed PEC biosensor owned outstanding stability. Moreover, the analysis device was tested under 10 times consecutive light "on/off" cycles to evaluate its repeatability. As shown in Fig. S4, the photocurrent response changed faintly and the relative standard deviation measured (RSD) was 9.49%, which indicated that the PEC biosensor had the distinguished reproducibility. Compared with other methods Table S2, the proposed sensor has the advantages of wide detection range and low detection limit.

4. Conclusions

In brief, a PEC biosensor based on cascaded amplified CdS/h-BN photosensitive structure was developed, which achieved ultrasensitive and specific detection of miRNA-141 through CHA mediated multipoint triggered DNA walker. The proposed platform possessed several prominent advantages: Primarily, the two-dimensional lamellar structure of h-BN loaded a large number of CdS QDs, which further provided sufficient active sites for biological reactions while stepping up the photocurrent signal. Then, the carefully designed three-point coordinated trigger TDW did not require the complex process of anchoring legs to orbit or Au NPs, simplifying procedures and increasing efficiency. Finally, the proposed PEC biosensor overcame the shortcomings of enzyme-assisted amplification to improve the sensitivity and specificity of analysis. More importantly, the developed PEC biosensor readily extended for a variety of other biomolecules detection, implying its great practical applications in biological analysis and early disease diagnosis.

CRediT authorship contribution statement

Fengyi Wang: Investigation, Methodology, Data curation, Writing – original draft. **Yaqi Liu:** Conceptualization, Methodology. **Lu Zhang:** Investigation, Formal analysis. **Zuhao Zhang:** Resources, Cooperation. **Chuan Huang:** Visualization, Data curation. **Dejin Zang:** Direction, Validation. **Haiqing Wang:** Validation, Supervision. **Shenguang Ge:** Conceptualization, Supervision, Funding acquisition. **Jinghua Yu:** Funding acquisition, Project administration.

Declaration of competing interest

The authors declare that they have no known competing financial interests or personal relationships that could have appeared to influence the work reported in this paper.

Data availability

No data was used for the research described in the article.

Acknowledgments

This work was supported by the National Natural Science Foundation of China (22074053, 21874055); Excellent Youth Innovation Team in Universities of Shandong (2019KJC016); The Project of "20 items of University" of Jinan (2020GXRC047); the Major Scientific and Technological Innovation Project of Shandong Province (2021CXGC010603); the Taishan Scholars program and Case-by-Case Project for Top Outstanding Talents of Jinan.

Appendix A. Supplementary data

Supplementary data to this article can be found online at https://doi.org/10.1016/j.aca.2022.340265.

References

[1] L. Li, Y. Zhang, Z. Yan, M. Chen, L. Zhang, P. Zhao, J. Yu, Ultrasensitive photoelectrochemical detection of microRNA on paper by combining a cascade nanozyme-engineered biocatalytic precipitation reaction and target-triggerable DNA motor, ACS Sens. 5 (2020) 1482–1490.
[2] H. Dong, J. Lei, L. Ding, Y. Wen, H. Ju, X. Zhang, MicroRNA: function, detection, and bioanalysis, Chem. Rev. 113 (2013) 6207–6233.
[3] L. Lu, D. Tu, Y. Liu, S. Zhou, W. Zheng, X. Chen, Ultrasensitive detection of cancer biomarker microRNA by amplification of fluorescence of lanthanide nanoprobes, Nano Res. 11 (2017) 264–273.
[4] J. Zhao, C. Fu, C. Huang, S. Zhang, F. Wang, Y. Zhang, L. Zhang, S. Ge, J. Yu, Co_3O_4-Au polyhedron mimic peroxidase- and cascade enzyme-assisted cycling process-based photoelectrochemical biosensor for monitoring of miRNA-141, Chem. Eng. J. 406 (2021) 1385–8947.
[5] C.S. Fang, K.S. Kim, B. Yu, S. Jon, M.S. Kim, H. Yang, Ultrasensitive electrochemical detection of miRNA-21 using a Zinc finger protein specific to DNA-RNA hybrids, Anal. Chem. 89 (2017) 2024–2031.
[6] Z. Chen, Y. Xie, W. Huang, C. Qin, A. Yu, G. Lai, Exonuclease-assisted target recycling for ultrasensitive electrochemical detection of microRNA at vertically aligned carbon nanotubes, Nanoscale 11 (2019) 11262–11269.
[7] X. Peng, Z.B. Wen, P. Yang, Y.Q. Chai, W.B. Liang, R. Yuan, Biomimetic 3d DNA nanomachine via free DNA walker movement on lipid bilayers supported by hard SiO_2@CdTe nanoparticles for ultrasensitive microRNA detection, Anal. Chem. 91 (2019) 14920–14926.
[8] J.L. Liu, Z.L. Tang, J.Q. Zhang, Y.Q. Chai, Y. Zhuo, R. Yuan, Morphology-controlled 9,10-diphenylanthracene nanoblocks as electrochemiluminescence emitters for microRNA detection with one-step DNA walker amplification, Anal. Chem. 90 (2018) 5298–5305.
[9] J. Ge, C. Li, Y. Zhao, X. Yu, G. Jie, Versatile "on-off" biosensing of thrombin and miRNA based on Ag(I) ion-enhanced or Ag nanocluster-quenched electrochemiluminescence coupled with hybridization chain reaction amplification, Chem. Commun. 55 (2019) 7350–7353.
[10] X. Li, H. Zhang, Y. Tang, P. Wu, S. Xu, X. Zhang, A both-end blocked peroxidase-mimicking dnazyme for low-background chemiluminescent sensing of miRNA, ACS Sens. 2 (2017) 810–816.
[11] P. Lavaee, S.M. Taghdisi, K. Abnous, N.M. Danesh, L.H. Khayyat, S.H. Jalalian, Fluorescent sensor for detection of miR-141 based on target-induced fluorescence enhancement and picogreen, Talanta 202 (2019) 349–353.
[12] H. Cui, B. Bo, J. Ma, Y. Tang, J. Zhao, H. Xiao, A target-responsive liposome activated by catalytic hairpin assembly enables highly sensitive detection of tuberculosis-related cytokine, Chem. Commun. 54 (2018) 4870–4873.
[13] Y. Li, S. Yue, H. Qi, C. Ding, W. Song, S. Bi, Target-triggered dynamic hairpin assembly for signal amplification of microRNA and oncogenes and its application in live-cell imaging, Chem. Commun. 55 (2019) 4103–4106.
[14] M. Hao, P. Miao, Y. Wang, W. Wang, S. Ge, X. Yu, X.X. Hu, B. Ding, J. Zhang, M. Yan, Near-infrared light-initiated photoelectrochemical biosensor based on upconversion nanorods for immobilization-free miRNA detection with double signal amplification, Anal. Chem. 93 (2021) 11251–11258.
[15] X. Niu, Y. Zhao, F. Wang, J. Wu, F. Qu, W. Tan, Ultrasensitive photoelectrochemical biosensor based on novel Z-scheme heterojunctions of Zn-defective CdS/ZnS for microRNA assay, Anal. Chem. 93 (2021) 17134–17140.
[16] Q. Zhang, S. Liu, C. Du, Y. Fu, K. Xiao, X. Zhang, J. Chen, Highly selective and sensitive microRNA-210 assay based on dual-signaling electrochemical and photocurrent-polarity-switching strategies, Anal. Chem. 93 (2021) 14272–14279.
[17] Z. Li, H. Yang, M. Hu, L. Zhang, S. Ge, K. Cui, J. Yu, Cathode photoelectrochemical paper device for microRNA detection based on cascaded photoactive structures and hemin/Pt nanoparticle-decorated DNA dendrimers, ACS Appl. Mater. Interfaces 12 (2020) 17177–17184.
[18] W.W. Zhao, J.J. Xu, H.Y. Chen, Photoelectrochemical bioanalysis: the state of the art, Chem. Soc. Rev. 44 (2015) 729–741.
[19] M.H. Zhu, X.M. Mu, H.M. Deng, X. Zhong, R. Yuan, Y.L. Yuan, Ultrasensitive photoelectrochemical biosensor for miRNA-21 assay based on target-catalyzed hairpin assembly coupled with distance-controllable multiple signal amplification, Chem. Commun. 55 (2019) 9622–9625.
[20] J. Shu, D. Tang, Recent advances in photoelectrochemical sensing: from engineered photoactive materials to sensing devices and detection modes, Anal. Chem. 92 (2020) 363–377.
[21] J. Tan, B. Peng, L. Tang, G. Zeng, Y. Lu, J. Wang, X. Ouyang, X. Zhu, Y. Chen, H. Feng, CuS QDs/Co_3O_4 polyhedra-driven multiple signal amplifications activated h-BN photoeletrochemical biosensing platform, Anal. Chem. 92 (2020) 13073–13083.
[22] J. Tan, B. Peng, L. Tang, C. Feng, J. Wang, J. Yu, X. Ouyang, X. Zhu, Enhanced photoelectric conversion efficiency: a novel h-BN based self-powered photoelectrochemical aptasensor for ultrasensitive detection of diazinon, Biosens, Bioelectron 142 (2019) 111546–111556.
[23] R. Kumar, S. Sahoo, E. Joanni, R.K. Singh, R.M. Yadav, R.K. Verma, D.P. Singh, W. K. Tan, A. Pérez del Pino, S.A. Moshkalev, A. Matsuda, A review on synthesis of graphene, h-BN and MoS_2 for energy storage applications: recent progress and perspectives, Nano Res. 12 (2019) 2655–2694.
[24] Y. Liu, K. Yan, J. Zhang, Graphitic carbon nitride sensitized with cds quantum dots for visible-light-driven photoelectrochemical aptasensing of tetracycline, ACS Appl. Mater. Interfaces 8 (2016) 28255–28264.
[25] S. Lv, K. Zhang, Y. Zeng, D. Tang, Double photosystems-based 'Z-scheme' photoelectrochemical sensing mode for ultrasensitive detection of disease biomarker accompanying three-dimensional DNA walker, Anal. Chem. 90 (2018) 7086–7093.
[26] J. Wang, D.X. Wang, A.N. Tang, D.M. Kong, Highly integrated, biostable, and self-powered DNA motor enabling autonomous operation in living bodies, Anal. Chem. 91 (2019) 5244–5251.
[27] T. Chen, Y. Chen, H. Chen, F. Zhang, Q. Zhang, G. Chen, X. Zhu, Dual-enzyme-propelled unbounded DNA walking nanomachine for intracellular imaging of lowly expressed microRNA, Nano Res. 12 (2019) 1055–1060.
[28] W.W. Zhao, J.J. Xu, H.Y. Chen, Photoelectrochemical DNA biosensors, Chem. Rev. 114 (2014) 7421–7441.
[29] M. Xu, D. Tang, Recent advances in DNA walker machines and their applications coupled with signal amplification strategies: a critical review, Anal. Chim, Acta 1171 (2021), 338523–338516.
[30] J. Chen, Z. Luo, C. Sun, Z. Huang, C. Zhou, S. Yin, Y. Duan, Y. Li, Research progress of DNA walker and its recent applications in biosensor, TrAC Trend, Anal. Chem. 120 (2019) 115626–116640.
[31] L. Wang, P. Liu, Z. Liu, K. Zhao, S. Ye, G. Liang, J.J. Zhu, Simple tripedal DNA walker prepared by target-triggered catalytic hairpin assembly for ultrasensitive electrochemiluminescence detection of microRNA, ACS Sens. 5 (2020) 3584–3590.
[32] K. Zhang, S. Lv, Z. Lin, M. Li, D. Tang, Bio-bar-code-based photoelectrochemical immunoassay for sensitive detection of prostate-specific antigen using rolling circle amplification and enzymatic biocatalytic precipitation, Biosens. Bioelectron. 101 (2018) 159–166.
[33] K. Zhang, S. Lv, M. Lu, D. Tang, Photoelectrochemical biosensing of disease marker on p-type Cu-doped $Zn_{0.3}Zd_{0.7}S$ based on RCA and exonuclease III amplification, Biosens. Bioelectron. 117 (2018) 590–596.
[34] R. Zeng, L. Zhang, L. Su, Z. Luo, Q. Zhou, D. Tang, Photoelectrochemical bioanalysis of antibiotics on RGO-Bi_2W_{06}-Au based on branched hybridization chain reaction, Biosens. Bioelectron. 133 (2019) 100–106.
[35] Y. Wang, Y. Wang, S. Liu, W. Sun, M. Zhang, L. Jiang, M. Li, J. Yu, J. Huang, Toehold-mediated DNA strand displacement-driven super-fast tripedal DNA walker for ultrasensitive and label-free electrochemical detection of ochratoxin a, Anal. Chim. Acta 1143 (2021) 21–30.
[36] W.W. Zhan, Q. Kuang, J.Z. Zhou, X.J. Kong, Z.X. Xie, L.S. Zheng, Semiconductor@metal-organic framework core-shell heterostructures: a case of ZnO@ZIF-8 nanorods with selective photoelectrochemical response, J. Am. Chem. Soc. 135 (2013) 1926–1933.
[37] Y. Fu, K. Zou, M. Liu, X. Zhang, C. Du, J. Chen, Highly selective and sensitive photoelectrochemical sensing platform for VEGF165 assay based on the switching of photocurrent polarity of CdS QDs by porous Cu_2O-CuO flower, Anal. Chem. 92 (2020) 1189–1196.
[38] Q. Zhang, Y. Fu, K. Xiao, C. Du, X. Zhang, J. Chen, Sensitive dual-mode biosensors for CYFRA21-1 assay based on the dual-signaling electrochemical ratiometric strategy and "on-off-on" PEC method, Anal. Chem. 93 (2021) 6801–6807.
[39] C. Feng, L. Tang, Y. Deng, G. Zeng, J. Wang, Y. Liu, Z. Chen, J. Yu, J. Wang, Enhancing optical absorption and charge transfer: synthesis of S-doped h-BN with tunable band structures for metal-free visible-light-driven photocatalysis, Appl. Catal. B Environ. 256 (2019) 117827–117836.